frontiers in Earth Science

ORIGINAL RESEARCH
published: 01 December 2021
doi: 10.3389/feart.2021.737995

Mechanism of Rock Bursts Induced by the Synthetic Action of "Roof Bending and Rock Pillar Prying" in Subvertical Extra-Thick Coal Seams

Zhenhua Wu[1,2], *Peng-Zhi Pan*[1,2]*, *Jianqiang Chen*[3], *Xudong Liu*[3], *Shuting Miao*[1,2] and *Peiyang Yu*[1,2]

[1]State Key Laboratory of Geomechanics and Geotechnical Engineering, Institute of Rock and Soil Mechanics, Chinese Academy of Sciences, Wuhan, China, [2]University of Chinese Academy of Sciences, Beijing, China, [3]Shenhua Xinjiang Energy Company Limited, Urumqi, China

OPEN ACCESS

Edited by:
Jie Chen,
Chongqing University, China

Reviewed by:
Xuesheng Liu,
Shandong University of Science and Technology, China
Mingzhong GAO,
Sichuan University, China
Huafu Qiu,
Xi'an University of Science and Technology, China

***Correspondence:**
Peng-Zhi Pan
pzpan@whrsm.ac.cn

Specialty section:
This article was submitted to Geohazards and Georisks, a section of the journal Frontiers in Earth Science

Received: *08 July 2021*
Accepted: *01 November 2021*
Published: *01 December 2021*

Citation:
Wu Z, Pan P-Z, Chen J, Liu X, Miao S and Yu P (2021) Mechanism of Rock Bursts Induced by the Synthetic Action of "Roof Bending and Rock Pillar Prying" in Subvertical Extra-Thick Coal Seams. Front. Earth Sci. 9:737995. doi: 10.3389/feart.2021.737995

When studying the rock burst mechanism in subvertical extra-thick coal seams in the Wudong coal mine in Xinjiang, China, most studies focus on rock pillars, while the effect of the roof on rock bursts is usually ignored. In this paper, a rock burst mechanism in subvertical extra-thick coal seams under the control of a "roof-rock pillar" is proposed. A theoretical analysis is first performed to explain the effect of roof-rock pillar combinations on rock bursts in coal seams. Numerical modeling and microseismic analysis are implemented to further study the mechanism of rock burst. The main conclusions are as follows: 1) During the mining of the B3+6 coal seam, an obvious microseismic concentration phenomenon is found in both the roof and rock pillar of B3+6. The rock bursts exhibited obvious directionality, and its main failure characteristics are floor heave and sidewall heave, but there will also be some failures such as shoulder socket subsidence in some parts. 2) The stress transfer caused by rock pillar prying is the main reason for the large difference in rock burst occurrence near the vertical and extra thick adjacent coal seams under the same mining depth. 3) Under the same cantilever length, the elastic deformation energy of the roof is much greater than that of the rock pillar, which makes it easier to produce high-energy microseismic events. With an increasing mining depth, the roof will become the dominant factor controlling the occurrence of rock bursts. 4) The high-energy event produced by the rock mass fracture near the coal rock interface easily induces rock bursts, while the high-energy event produced by the fracture at the far end of the rock mass is less likely to induce rock burst. 5) Roof deformation extrusion and rock pillar prying provide high static stress conditions for the occurrence of rock bursts in the B3+6 coal seam. The superposition of the dynamic disturbance caused by roof and rock pillar failure and the high static stress of the coal seam is the main cause of rock burst in the B3+6 coal seam.

Keywords: rock bursts, subvertical extra-thick coal seams, adjacent coal seams, roof bending, rock pillar prying

INTRODUCTION

Rock bursts are dangerous phenomena caused by the brittle failure of deep rock and are associated with excavation-induced seismic events (Kaiser and Cai, 2013). The occurrence of rock bursts usually causes significant economic losses, such as equipment damage and construction delays, and even worker injuries (He, 2011; Feng et al., 2012; Mazaira and Konicek, 2015; Lu et al., 2016; Dou et al., 2018; Feng et al., 2019; Naji et al., 2019; Simser, 2019; Wang et al., 2020; Wu et al., 2021a). They are one of the common dynamic instability modes during underground mining and excavation in the hardness, brittleness and integrity surrounding rock strata. In many cases, a rock burst in a coal mine can destroy tunnels hundreds of meters long, causing equipment damage and casualties (Aydan et al., 2002; Zhu et al., 2015; Afraei et al., 2019). The scale and severity of the damage in coal mines are usually greater than those in hard rock engineering.

Steeply inclined coal seams are widely distributed in Xinjiang, Ningxia, and Gansu in China, Asturias in Spain, and Lorraine in France, as well as other coal-producing regions (Diez and Alvarez, 2000; Driad-Lebeau et al., 2005; Heib, 2012; Qi et al., 2019b; He et al., 2020b). The steeply dipping thick coal seam contributes to approximately 17% of the total coal reserve and 10% of the total coal production of China (Duan et al., 2008; Wu et al., 2014). In recent years, as the mining intensity has increased, some areas in the east have suffered from the depletion of coal reserves that have had good conditions for many years. Many mining areas have begun to consider the mining of steep coal seams distributed in the west. However, compared with a gently inclined coal seam, the roof of a steeply inclined coal seam is not located above the stope but at the side of the stope. Therefore, the stress environment of steeply inclined coal seam roofs, the movement characteristics of overburden and the fracture mechanism are obviously different from those of gently inclined coal seams (Unver and Yasitli, 2006; Miao et al., 2011; Lai et al., 2014). The subvertical extra-thick coal seam is a type of coal seam with a large dip angle of 85–90° and is recognized as difficult to mine in academic circles (Lai et al., 2014; Lai et al., 2018). Because of their special characteristics of a high horizontal stress and complex geological conditions, the critical depth for rock bursts is less than that of most coal mines. The mine area of Urumchi has more than 30 steeply dipping coal seams with various thicknesses and spacings. Among them, the south mining area of the Wudong Coal Mine has particularities in addition to the special occurrence of the steeply dipping thick coal seam. In the southern area of the Wudong coal mine, an ultrathick rock pillar occurs between adjacent coal seams of the steeply dipping coal seam group. It has been shown that when the adjacent working face is mined, the complete and hard thick rock layer plays a macrocontrol role on the working face pressure, and the coupling effect of the stress transfer and structural stress of the thick rock layer increases the static load and the accumulation of the coal and rock mass, which provides the force source conditions for a rock burst occurrence (Xu et al., 2015; Liu et al., 2017; Qi et al., 2019a). Under the coupling action of suspended roofs and rock pillars, adjacent mining faces with the same mining depth may show completely different rock burst behaviors due to the asymmetry of deformation, failure, energy, and stress transfer of the two working faces. Some experts have been investigated the rock burst mechanisms in steeply inclined coal mines with such coal and rock occurrences and mining conditions, and some meaningful results are obtained (Li et al., 2020a; Wu et al., 2021b; He et al., 2021). However, most studies are based on numerical simulation, and lack of relevant theoretical analysis. Therefore, it is of great significance to analyze the mechanism of rock burst with a combination of theoretical analysis and numerical simulation. Compared with gently inclined coal seams, research on the rock burst mechanism of subvertical extra-thick coal seams is immature. Research on subvertical extra-thick coal seams is rarely reported and is still in the exploratory stage.

Rock bursts are usually induced by a combination of dynamic and static loads (Cai et al., 2020; Cao et al., 2020). However, the sources of a dynamic load and static stress and the mechanism of a rock burst in the process of mining are still unclear for this special geological structure coal seam. Due to the particularity of the geological structure of subvertical extra-thick coal seams, the occurrence of rock bursts in adjacent coal seams with the same mining depth in the same mining area is different. Currently, some studies are focused on the deformation and failure of roadways under the control of rock pillars. Although the impact of roof on rock burst is considered by some scholars, it is limited to numerical simulations (Li et al., 2020a; He et al., 2021).

In this paper, mechanical models of roof and rock pillar are established based on the Wudong coal mine in Urumqi, Xinjiang. The change law of elastic deformation energy of a roof and rock pillar with an increase in the mining depth and its effect on rock burst in B3+6 coal seam are obtained, and the reason that a rock burst does not occur in the adjacent B1+2 coal seam is explained. Based on numerical modeling and microseismic monitoring, the sources of the dynamic loads and static stress are determined, and the mechanism of rock burst under the joint mining condition of adjacent subvertical extra-thick coal seams is systematically analyzed.

ENGINEERING BACKGROUND

Occurrence Characteristics of Rock Burst and Mining Conditions of the Coal Seam

This study case is located in the Urumqi mining area. Due to the strong geological movement, the dip angles of the north and south wings of the Badaowan syncline are approximately 87° and 45°, respectively. The southern area of the Wudong coal mine is located in the southern wing of the Badaowan syncline. The south mining area of the Wudong coal mine belongs to the near vertical extra-thick coal seam group. The main mining areas are B3+6 and B1+2. To meet the economic benefit requirements, an alternate production mode of two working faces is adopted, among which the B3+6 working face is the first mining face (**Figure 1**), and the tail entry and head entry are arranged along the roof and floor of the coal seam, respectively. The width of the working face is the

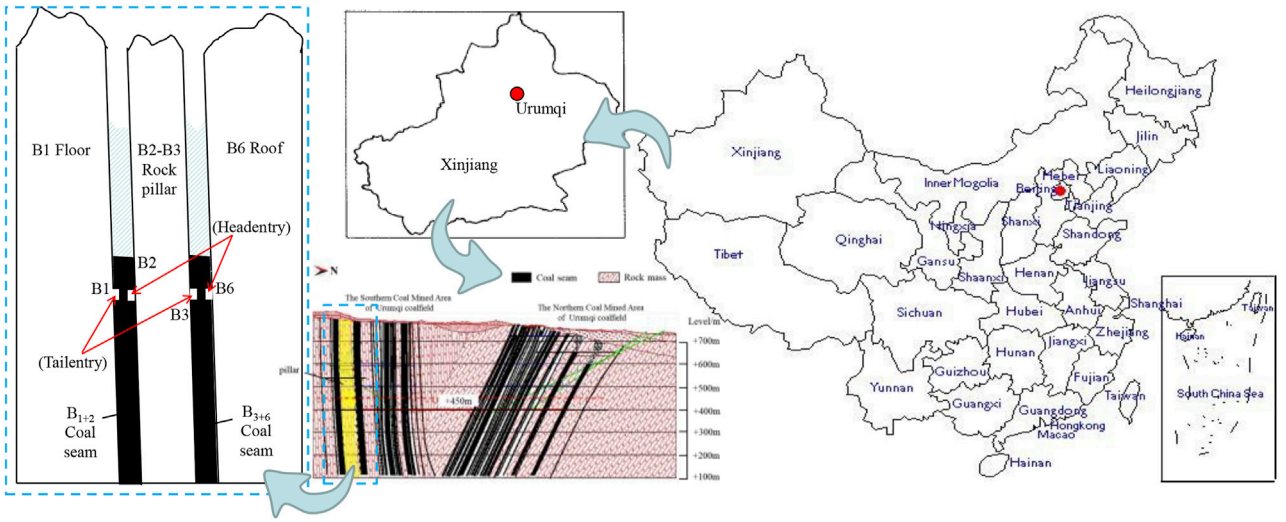

FIGURE 1 | Distribution and geological profile of northern and southern mining areas in the Urumqi mining area.

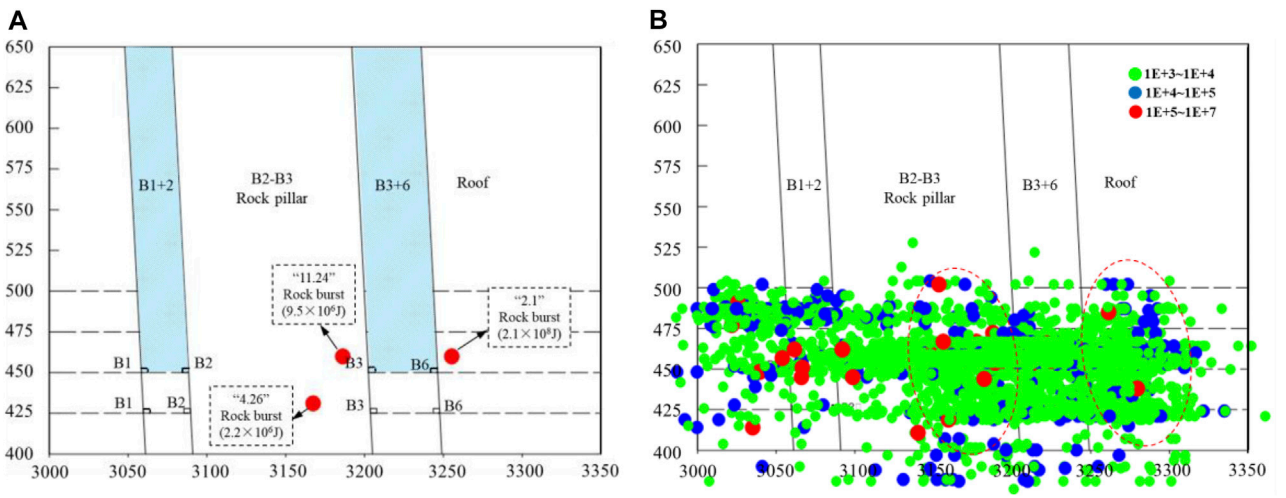

FIGURE 2 | Microseismic events distribution characteristics of rock bursts. **(A)** Elevation view of the rock burst distribution; **(B)** Spatial distribution of microseismic events with energy in the range of 10^3–10^7 J.

thickness of the coal seam, the height of the layer is 25 m, and the mining drawing ratio is approximately 1:7. The coal mine adopts single wing horizontal sublevel fully mechanized top coal caving technology, and the roof is managed by the natural caving method. The average thickness of the B1+2 coal seam is 37.45 m, that of the B3+6 coal seam is 48.87 m, and the strike length of both coal seams is 2,520 m. There are hard and thick rock pillars between the two coal seams, with an average thickness of 100 m. The results of the *in situ* stress test in the south mining area of the Wudong coal mine show that the horizontal stress σ_H is 1.9–2.2 times the vertical stress σ_V when the mining depth exceeds 300 m (Lai et al., 2015), which indicates that the horizontal stress is the main factor leading to the occurrence of rock bursts. According to the statistics of rock burst accidents in the southern mining area of the Wudong coal mine, the mining depth of the B3+6 coal seam in the southern mining area of the Wudong coal mine is approximately 300 m, which is far less than the critical depth of rock bursts in a gently inclined coal seam.

MS Monitoring System

The Wudong coal seam adopts the ARAMIS M/E MS monitoring system, which is capable of monitoring MS events (with an energy above 100 J, a frequency within 0–150 Hz, and an anti-interference ability lower than 100 dB) across the mine area, and the data can be used to effectively identify the areas at risk of rock burst (Xu et al., 2017). The Wudong coal mine south mining area adopts the joint monitoring of the surface and underground, which increases the positioning accuracy, to a certain extent.

According to field monitoring, three rock bursts occurred in the B3+6 coal seam at the +450 mining level. The occurrence locations of the three rock bursts are shown in **Figure 2A**, and the three events are named 11.24, 2.1, and 4.26 per their occurrence dates.

Field practice shows that microseismic events with energy levels greater than 10^6 J easily cause rock bursts in coal mines. This kind of microseismic event with a high risk of inducing rock bursts is called an "induced shock event" (He et al., 2017). During the mining process of the +450 horizontal coal seam, 22,649 microseismic spontaneous events were monitored, including 23 "induced shock events." According to a statistical analysis of the distribution of "induced scour events" in the mining process of the B3+6 coal seam, the regional distribution was very obvious, with 62.5% in the rock pillar, 25.0% in the B3+6 coal seam, and 12.5% in the roof of the B3+6 coal seam. According to the microseismic event energy in the range of 10^3 J~10^7 J, it can be determined that the microseismic events near the B3+6 coal seam are distributed intensively (**Figure 2B**) (red dotted line area). The distribution of micro earthquakes in the roof of the B3+6 coal seam also has a similar concentration area, and there are obviously more microseismic events in the B3+6 coal seam than in the B1+2 coal seam. This is because the hanging rock pillar and roof bend to one side of the goaf, and the coal body is squeezed by the rock pillar and roof together, resulting in an increase in the coal stress, which is more likely to produce high-energy events in the process of mining.

Description and Analysis of Rock Bursts

The positions of the three rock bursts are in the B3 and B6 roadways of the B3+6 coal seam, while the B1 and B2 roadways of the B1+2 coal seam are not affected at the same mining depth. The rock bursts exhibited obvious directionality. Based on the actual rock burst situation and the analysis of image data, it can be determined that there are obvious floor heave and sidewall heave deformations in B3 and B6, especially at the bottom corner of the south side of B3 where the floor heave deformation is more obvious, as well as a large top subsidence in B6, where the subsidence of the shoulder socket on north side is more serious. Combined with the damage of the roadway after rock burst and field microseismic monitoring data, it can be determined that there are two main reasons for the rock burst in the B3+6 coal seam:

1) With a continuous increase in the coal seam mining depth, the rock pillar between coal seams is in a state of suspension. Under the action of an external load and self-weight, the rock pillar moves to the goaf of the B1+2 coal seam and pries B3+6 coal seam to produce a stress transfer. The stress of the B1+2 coal seam transfers to the B3+6 coal seam through the rock pillar, which increases the probability of a rock burst in the B3+6 coal seam. However, the B1+2 coal seam with the same mining depth is not prone to rock bursts due to the release of coal seam stress.
2) In addition to the stress transfer of the rock pillar, the B3 + 6 roof is bent and deformed under the action of horizontal tectonic stress and overburden load, which compresses the coal body of the B3+6 coal seam, resulting in a large roof deformation of the roadway (especially B6) when rock burst occurs.

MECHANICAL ANALYSIS OF THE HARD ROOF AND HARD-ROCK PILLAR

According to the analysis above, rock pillar prying and roof bending and extrusion are the main reasons for the rocks bursts in the B3+6 coal seam. Therefore, it is necessary to establish mechanical models for roofs and rock pillars in order to analyze the control effect of rock bursts.

Theoretical Analysis of Rock Bursts Induced by Stress Transfer of Hard Rock Pillar

Taking the rock pillar and the coal seams on both sides in as the research object, the mechanical model is established (**Figure 3**). The rock pillar is simplified as a cantilever beam OB for the

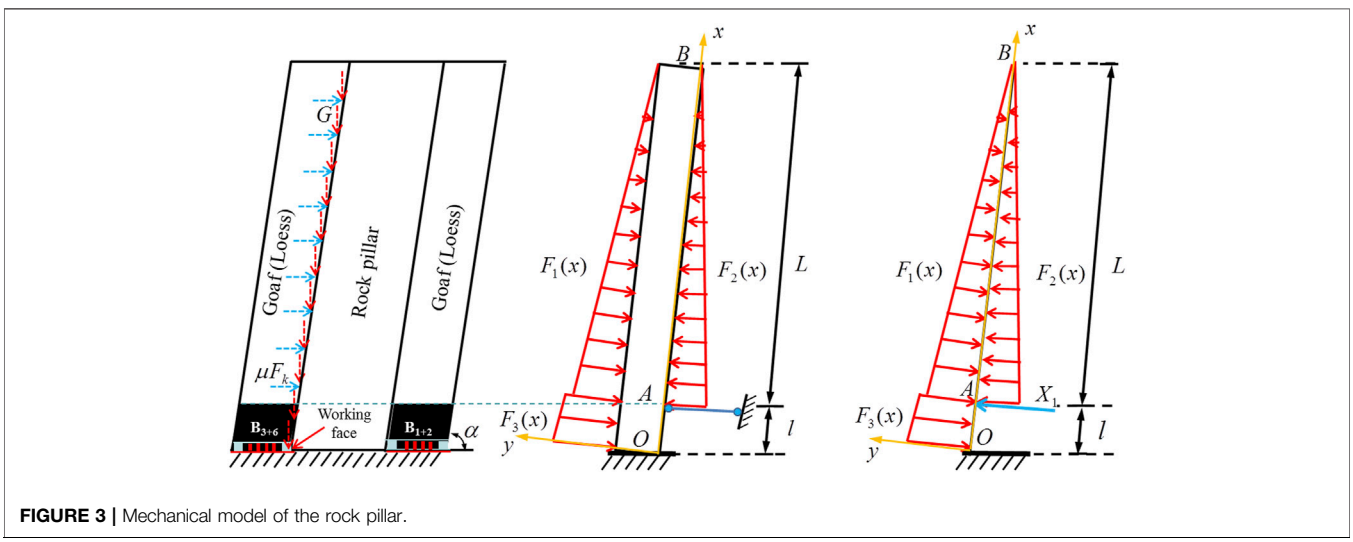

FIGURE 3 | Mechanical model of the rock pillar.

mechanical analysis. The cantilever length is L, the length of the constrained part is l, and the angle between the cantilever and the horizontal direction is α. The bottom of the rock pillar extends from the working face to the coal body. Under the joint action of the coal body and the overlying strata, the bottom constraint can be regarded as a fixed constraint. The coordinate system is then established with the bottom end point of the rock pillar as the origin, where x is the upward distance along the surface of the rock pillar. The residual stress μF_k after attenuation of the horizontal tectonic stress, the self-weight of loess and rock pillar, and the component force along the y-axis of the rock pillar are simplified as triangular load $F_1(x)$, and the axial load is ignored (the axial load does not lead to rock pillar bending). $F_3(x)$ is the binding force of the B3+6 coal body on the rock pillar. Combined with the actual conditions of the site, the following two points need to be explained:

1) Under actual mining conditions, the fully mechanized caving face is mined from east to west. In the process of mining, with an increasing mining distance, the binding force of coal on the rock mass gradually decreases;
2) In this model, B1+2 can alleviate the bending deformation of the rock pillar. To investigate the bending effect of the rock pillar, the force of the B1+2 coal seam on the rock pillar is simplified as a simply supported support, which acts at the junction of the coal seam and loess.

According to the study of *in situ* stress, the horizontal tectonic stress can be estimated according to the vertical stress, where the ratio of the horizontal tectonic stress to vertical stress is a. Assuming that the width of the rock pillar on any section is a unit length, the load on the rock pillar at any section can be deduced as follows:

$$F_1(x) = (L + l - x)\sin\alpha\left[\mu A\gamma_s \sin\alpha + (\gamma_L + \gamma_P)\cos\alpha\right] \quad (l \le x \le L + l) \tag{1}$$

where μ is the attenuation coefficient of the horizontal tectonic stress; γ_s is the average bulk density of overlying strata on the roof of the B3+6 coal seam; γ_L is the bulk density of backfill loess; γ_P is the bulk density of the rock pillar; and α is the dip angle of the coal seam.

Because the loess is loose, it is inevitable that the compactness of different positions is not consistent in the process of backfill, or the cavity, loess and rock pillar are not fully contacted. If the support effectiveness coefficient f is defined here, then the support force of loess to the rock pillar can be expressed as follows:

$$F_2(x) = \frac{1}{\lambda} f\gamma_L[(L + l) - x]\sin^2\alpha \quad (l \le x \le L + l) \tag{2}$$

where λ is the lateral pressure coefficient, $\lambda = 1/A$; and the value range of the support effectiveness coefficient f is [0,1]. Under the ideal filling condition, $f = 1$, but when the loess has no supporting effect on the rock pillar, $f = 0$.

When the B3+6 coal seam does not start mining, the binding force of the coal seam on the rock pillar is equal to the horizontal *in situ* stress. When the B3+6 coal seam starts mining, the binding force of the coal seam on the rock pillar is assumed to be k; then, the binding force of the B3+6 coal seam on the rock pillar can be expressed as:

$$F_3(x) = kA\gamma_s[(L + l) - x]\sin^2\alpha \quad (0 < x \le l) \tag{3}$$

where the constraint weakening coefficient $k = 1\text{-}L'/L$, L' is the length of the coal seam that has been mined, and L is the design strike length of the coal seam. When the coal seam is mined out, $k = 0$ (at this time, it is considered that it is the moment when the coal seam is just finished). Because the coal mining height is far less than the suspended length of the rock pillar, it is approximately regarded as a uniform load in a later calculation.

According to the idea of the "geometry, physics, balance" analysis of statically indeterminate problems in material mechanics, the force is taken as the basic unknown quantity, the structural body is analyzed based on automatically satisfying the equilibrium conditions, and the deformation coordination of the cantilever structure is mainly considered. The redundant restraint is removed and the excess reaction force and load are retained. If the load is the same and the excess reaction force is equal to the actual force, then the stress state of the cantilever beam is exactly the same, and the deformation and displacement of the original structure and the basic system are also identical. For j-order statically indeterminate structures, the equation after removing redundant constraints can be written as follows:

$$\begin{cases} \delta_{11}X_1 + \delta_{12}X_2 + \cdots\delta_{1i}X_i + \cdots\delta_{1j}X_j + \Delta_{1P} = 0 \\ \delta_{21}X_1 + \delta_{22}X_2 + \cdots\delta_{2i}X_i + \cdots\delta_{2j}X_j + +\Delta_{2P} = 0 \\ \vdots \\ \delta_{i1}X_1 + \delta_{i2}X_2 + \cdots\delta_{ii}X_i + \cdots\delta_{ij}X_j + +\Delta_{iP} = 0 \\ \vdots \\ \delta_{j1}X_1 + \delta_{j2}X_2 + \cdots\delta_{ji}X_i + \cdots\delta_{jj}X_j + +\Delta_{jP} = 0 \end{cases} \tag{4}$$

where δ_{ij} is the generalized displacement caused by the generalized force at j in the direction of x_i, and Δ_{iP} is the displacement caused by the actual external load in the direction of x_{ij}. δ_{ij} and Δ_{iP} are called the displacement influence coefficient (flexibility coefficient) and the free term, respectively. The calculation method is shown in **Eq. 5** and **Eq. 6**.

$$\delta_{ij} = \sum\int \frac{\bar{M}_i\bar{M}_j}{EI}ds \tag{5}$$

$$\Delta_{iP} = \sum\int \frac{\bar{M}_iM_P}{EI}ds \tag{6}$$

Writing **Eq. 4** as a matrix:

$$[\delta]\{X\} + \{\Delta\} = \{0\} \tag{7}$$

where $[\delta]$ is the structural flexibility matrix, X is the free term matrix of the structure, and Δ is the force matrix to be solved.

The constraint of the B1+2 coal seam on the rock pillar at point A is released, and the constraint reaction force X_1 is applied. The deformation coordination condition is that the deflection at point A is 0. Taking $F_1(x)$, $F_2(x)$, $F_3(x)$, and X_1 into **Eq. 5** and **Eq. 6**, the flexibility coefficient and the free term under different loads

TABLE 1 | Bending moment diagram of the rock pillar's basic structure under different loads.

	M_{F1}	M_{F2}	M_{F3}	M_{X1}
Basic structure	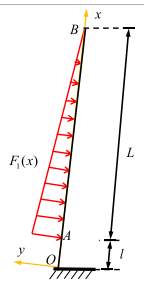	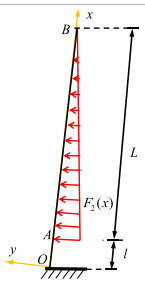	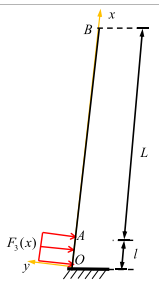	
δ_{ij}	—	—	—	$\frac{l^3}{3EI}$
Δ_{iP}	$\frac{-q_1 L^2 l^2}{12EI}$	$\frac{q_2 L^2 l^2}{12EI}$	$\frac{-q_3 l^4}{8EI}$	—

Notes $q_1 = \mu A \gamma_s L \sin^2\alpha + (\gamma_L + \gamma_P) L \sin\alpha \cos\alpha$; $q_2 = f\gamma_L \lambda^{-1} L \sin^2\alpha$; $q_3 = kA\gamma_s L \sin^2\alpha$.

can be obtained. The results are shown in **Table 1** (only an approximate calculation is made in the table).

The binding force of the B1+2 coal seam on the rock pillar can be obtained by taking the calculation results in **Table 1** into **Eq. 7**.

$$X_1 = \frac{(q_1 - q_2)L^2}{4l} + \frac{3q_3 l}{8} \tag{8}$$

When the local stress conditions and physical and mechanical parameters of loess are known, q_1 and q_2 in **Eq. 8** are constant values. With mining of the B3+6 coal seam, the binding force q_3 of the B3+6 coal seam on the rock pillar gradually decreases. According to Newton's third law, the pressure of the rock pillar on the B1+2 coal seam gradually decreases. In short, the mining of the B3+6 coal seam has a pressure relief effect on the B1+2 coal seam, which reduces the probability of a rock burst in the B1+2 coal seam, to a certain extent.

The suspended rock pillar will inevitably bend and deform. Assuming that the bending stiffness of the suspended rock pillar is constant, then the approximate differential equation of the deflection curve of the rock pillar can be expressed as follows:

$$EI\omega = -\int\left[\int M(x)dx\right]dx + C_1 x + C_2 \tag{9}$$

where C_1 and C_2 are integral constants, which are determined by the boundary conditions of the deflection curve of the beam, and $M(x)$ is the bending moment equation of the beam.

The deflection change of the rock pillar's OA section has a direct impact on the mining of the B3+6 coal seam. According to the superposition principle, the deflection curve equation of the rock pillar OA section can be obtained:

$$\omega(x) = \frac{(q_1 - q_2)L^2 x^2}{24EI}(1 - xl) + \frac{q_3 x^2}{48EI}(-2x^2 + 5lx - 3l^2) \quad (0 < x \le l) \tag{10}$$

Because the variation range of the parameters, such as the density of overlying strata and the density of backfill loess, is small, the paper considers that the material parameters at different positions are essentially the same, and the single parameter method is used to analyze the variation of the deflection of a rock pillar with k in the OA section. According to the field measurement results, the default values of the expression parameters are set as follows: γ_s = 29.82 KN/m^3; γ_P = 24.83 KN/m^3; γ_L = 16.2 KN/m^3; E = 26.63 GPa; A = 2; λ = 0.5; f = 0.85; α = 87°; and k = 0.5. By substituting the above parameters

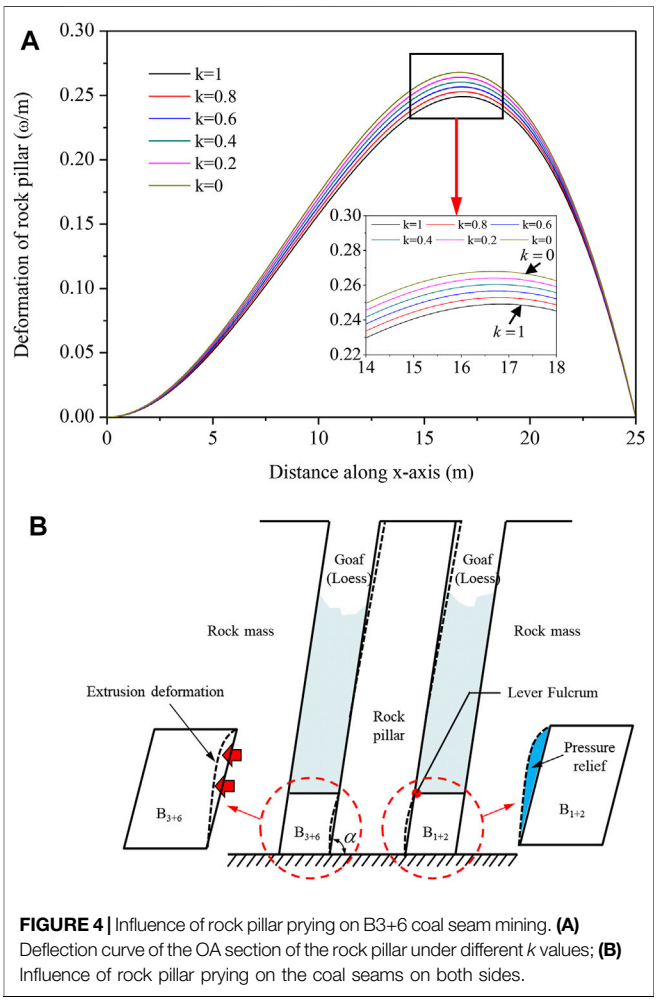

FIGURE 4 | Influence of rock pillar prying on B3+6 coal seam mining. **(A)** Deflection curve of the OA section of the rock pillar under different k values; **(B)** Influence of rock pillar prying on the coal seams on both sides.

into **Eq. 10**, the deflection curves of the OA section of the rock pillar under different k values are obtained (assuming that the deflection changes to the B3+6 coal seam are positive).

As seen from **Figure 4A**, with a decrease in the constraint weakening coefficient k, the deformation of the OA section of the rock pillar increases, especially in the range of 12–18 m above the working face, and the rock pillar crowing is more obvious. This is mainly because with the continuous extraction of the coal body in the B3+6 coal seam, the binding force of the coal body on the rock pillar is gradually reduced, and the activation degree of the rock pillar is strengthened, leading to a more obvious prying action. The rock pillar takes the coal body of coal seam B1+2 as the fulcrum and deflects to the goaf of coal seam B1+2, releasing the stress of the coal body of coal seam B1+2. However, the stress of the coal body of coal seam B3+6 increases due to the extrusion effect, which increases the probability of a rock burst (**Figure 4B**). The stress transfer of the rock pillar caused by prying is the main reason for the difference in rock bursts in adjacent coal seams with the same mining depth.

According to the load distribution, the moment function $M(x)$ along the rock pillar can be calculated, and then the deformation energy of the rock pillar at any position can be obtained. The bending moment at any position of the rock pillar is:

$$M(x)=\begin{cases}\dfrac{\left[\mu A\gamma_s-f\gamma_L\lambda^{-1}+(\gamma_L+\gamma_P)\cos\alpha\right]L^2\sin^2\alpha}{4l}\left[(L-2l)x+2l^2-\dfrac{1}{3}Ll\right]\\ \qquad+\dfrac{kA\gamma_sL\sin^2\alpha}{8}(l-x)(l-4x)\\ \qquad(0\le x\le l)\\ \dfrac{(L+l-x)\sin^2\alpha\left[\mu A\gamma_s+(\gamma_L+\gamma_P)\cos\alpha-f\gamma_L\lambda^{-1}\right]}{6}(L+l-x)^2\\ \qquad(l<x\le L+l)\end{cases}\tag{11}$$

According to the relationship between the bending moment and the elastic deformation energy, the elastic deformation energy at any x along the rock pillar can be expressed as:

$$U(x)=\begin{cases}\dfrac{1}{2EI}\left[\dfrac{\left[\mu A\gamma_s-f\gamma_L\lambda^{-1}+(\gamma_L+\gamma_P)\cos\alpha\right]L^2\sin^2\alpha}{4l}\left[(L-2l)x+2l^2-\dfrac{1}{3}Ll\right]+\right.\\ \left.\dfrac{kA\gamma_sL\sin^2\alpha}{8}(l-x)(l-4x)\right]^2\\ \qquad(0\le x\le l)\\ \dfrac{1}{2EI}\left[\dfrac{(L+l-x)\sin^2\alpha\left[\mu A\gamma_s+(\gamma_L+\gamma_P)\cos\alpha-f\gamma_L\lambda^{-1}\right]}{6}(L+l-x)^2\right]^2\\ \qquad(l\le x\le L+l)\end{cases}\tag{12}$$

Under the condition of different rock pillar suspension lengths L, the variation curve of the elastic deformation energy of the rock pillar along the coordinate axis x direction is shown in **Figure 5A**.

Figure 5A shows that the elastic deformation energy of the rock pillar increases with an increasing suspended height. At the junction of the coal seam and loess, the elastic deformation energy of the rock pillar reaches its maximum, and the rock pillar is most prone to fracturing. According to the statistical analysis of the high-energy microseismic events (>10^3 J) around the +450 mining horizontal pillar in the B3+6 coal seam (**Figures 5B–C**), it can be determined that 73.2% of the high-energy events are distributed in the range of 18–25 m above the working face (in particular, the high-energy events are more concentrated at approximately 22–23 m), which indicates that the rock pillar activity is more intense in this area. Because the theoretical calculation results are based on the assumption of idealized conditions, there will be some deviations from the actual conditions, but they are essentially consistent with the field

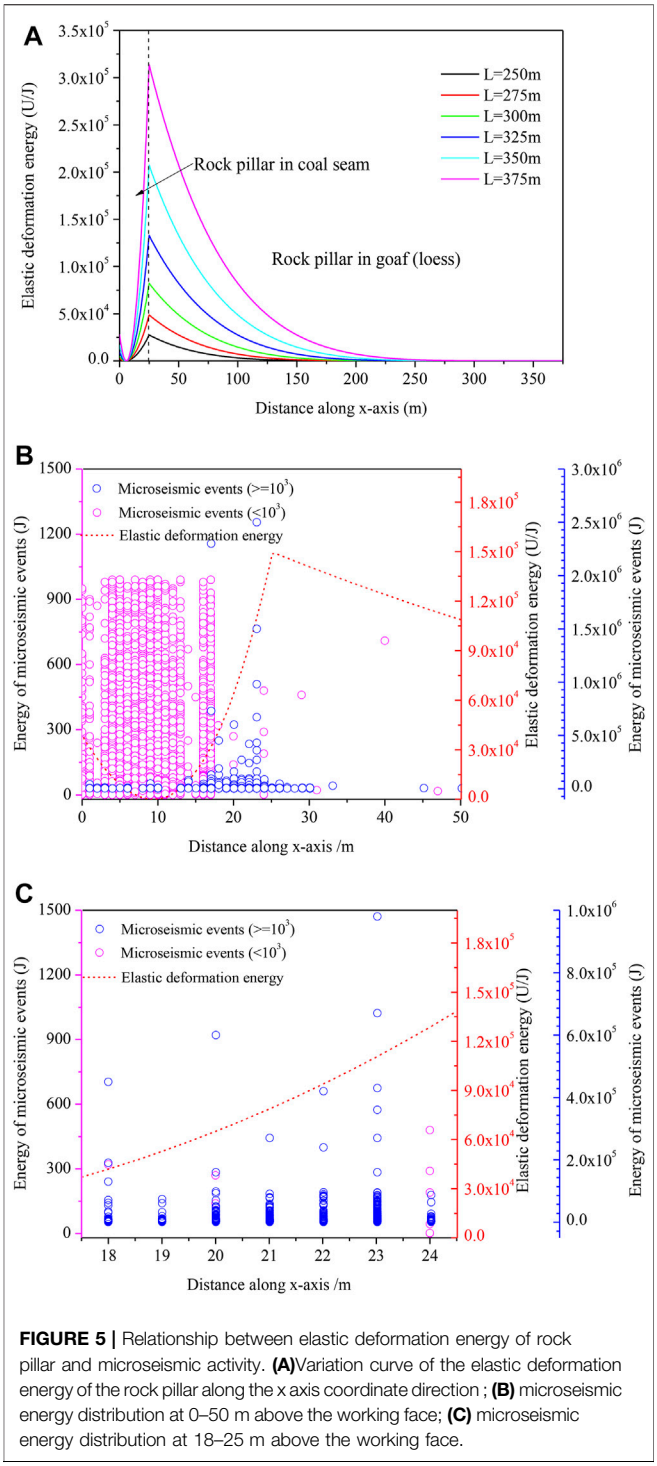

FIGURE 5 | Relationship between elastic deformation energy of rock pillar and microseismic activity. **(A)**Variation curve of the elastic deformation energy of the rock pillar along the x axis coordinate direction ; **(B)** microseismic energy distribution at 0–50 m above the working face; **(C)** microseismic energy distribution at 18–25 m above the working face.

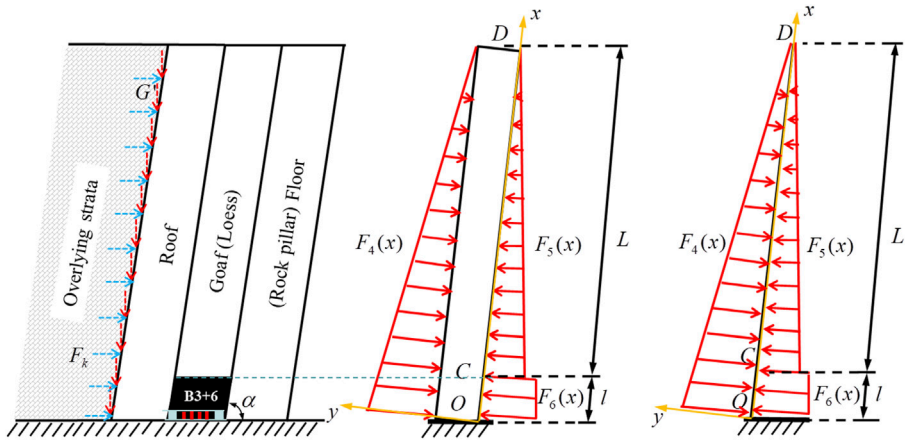

FIGURE 6 | Mechanical model of a rock pillar.

TABLE 2 | Bending moment diagram of the basic roof structure under different loads.

	M_{F4}	M_{F5}	M_{F6}
Basic structure	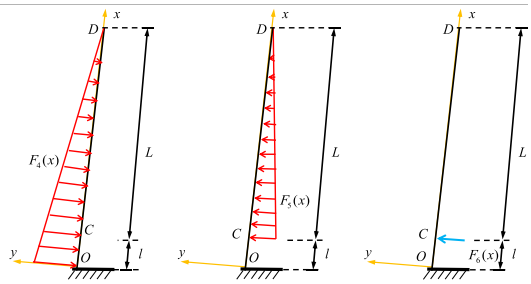		
δ_{ij}	—	—	$\frac{\beta}{3EI}$
Δ_{iP}	$\frac{-F_4(x)l^2}{12EI}(L+\frac{2}{3}l)^2$	$\frac{q_5L^2}{12EI}(L+2l)$	—

Notes $q_5 = \frac{1}{\lambda} f\gamma_L L\sin^2\alpha$.

monitoring results. The events near the working face are mainly low-energy position events, which are due to the compression of the rock pillar on the B3+6 coal seam, which leads to an increase in coal mining stress in this area. However, in the process of coal mining the coal body is constantly disturbed by an external load. In this process, a part of the coal body is released without storing high energy, which leads to more low-energy microseismic events.

A large amount of elastic deformation energy is stored in the rock pillar at the interface of the coal seam and loess. When the rock mass breaks a large amount of energy will be released. Because the distance between the fracture position of the rock pillar and coal seam is short, the seismic wave generated after the rock pillar fracture can act on the coal body quickly without great attenuation, resulting in a rapid increase in the coal stress and the superposition of dynamic stress and static stress. Therefore, B3+6 coal seam is prone to rock bursts. However, the elastic deformation energy of the rock pillar in the goaf area is small, and the rock pillar does not easily break. Even if fracture occurs, the dynamic stress applied to the coal body by seismic wave load disturbance action will be greatly reduced due to the attenuation of the long-distance transmission process. To more intuitively show the variation in the vibration wave load disturbance with distance, it is assumed that the rock pillar breaks at x m away from the coal rock interface, the vibration wave propagates vertically down to the coal body of the B3+6 coal seam along the shortest distance, and the mine earthquake energy is 1×10^6 J. The densities of the coal and rock mass are 1,325 and 2,663 kg/m^3, respectively, and the propagation velocities of the S-wave in intact sandstone are 4.2 and 2.4 km/s, respectively. One study (Wang et al., 2018) fitted and analyzed the *in situ* test data of the propagation law of underground vibration waves in coal mines and obtained the relationship between the peak vibration velocity of particles and the energy of mine earthquakes:

$$V_{pm} = 0.0645U_k^{0.3566} \tag{13}$$

where V_{pm} is the peak vibration velocity of the particle and U_{k} is the energy value of the microseismic event.

Assuming that coal is an isotropic continuous medium, the dynamic stress caused by the propagation of vibration waves to a specific position of the medium can be expressed as (Dou et al., 2014):

$$\begin{cases} \sigma_{dP} = 0.0645U_k^{0.3566}\rho_m C_{Pm}\prod_{i=1}^{n} L_i^{-\lambda_i} \\ \tau_{dS} = 0.0645U_k^{0.3566}\rho_m C_{Sm}\prod_{i=1}^{n} L_i^{-\lambda_i} \end{cases} \tag{14}$$

where σ_{dP} and τ_{dS} are the dynamic stresses produced by the P-wave and S-wave, respectively; ρ_m is the density of the medium at L_m away from the source boundary; C_{Pm} and C_{Sm} are the wave velocities of the P-wave and S-wave at L_m from the source boundary; L_i is the propagation distance of the seismic wave in the i-th medium, $L_m = \sum_{i=1}^{m} L_i$; m represents the m-th propagation medium; and λ_i is the attenuation coefficient of the i-th medium.

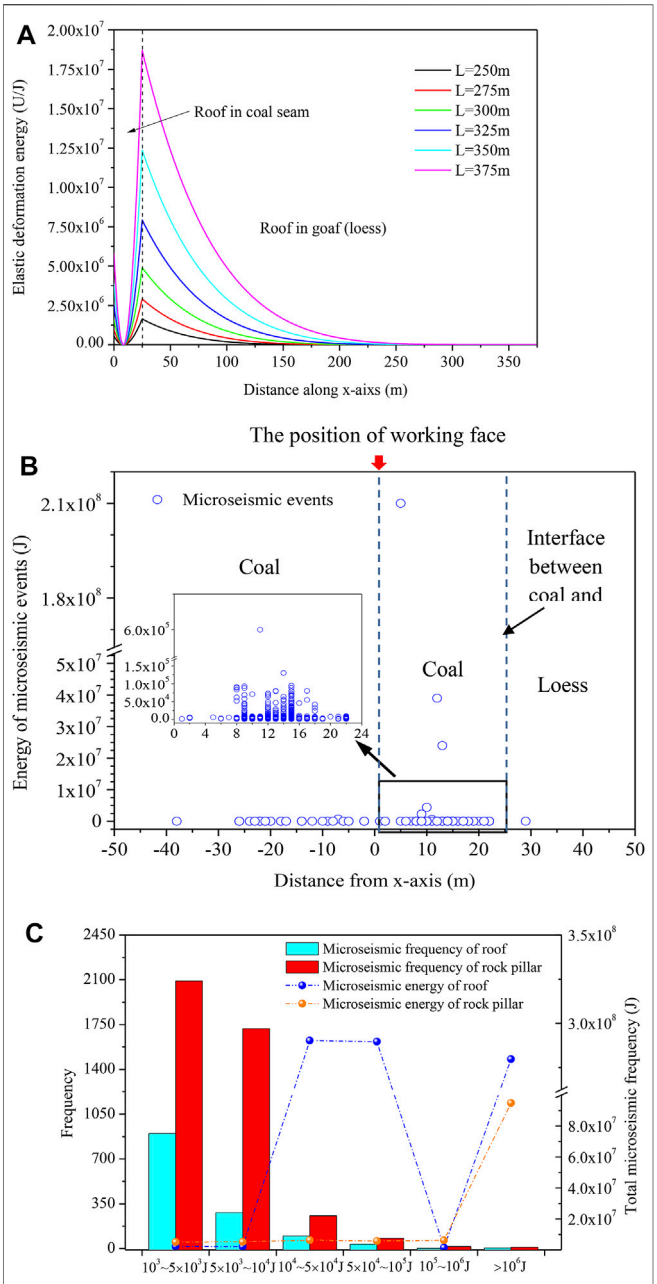

FIGURE 7 | Relationship between elastic deformation energy of roof and microseismic activity. **(A)** Variation curve of the elastic deformation energy of the roof along the coordinate axis x direction; **(B)** microseismic distribution at different positions of the roof ("0" is the position of the working face; "coal" refers to the roof in solid coal; "loess" refers to the suspended roof); **(C)** statistics of the energy and frequency of microseismic events in the B3+6 coal seam at the +450 m level.

He and Dou (2012) used a microseismic monitoring system and blasting to obtain the attenuation coefficient $\lambda = 1.526$. According to **Eq. 12**, the variation curve of the vibration wave generated using a rock pillar fracture with the distance calculated. The result of calculation showed that the initial propagation stage of the vibration wave attenuates the fastest before gradually

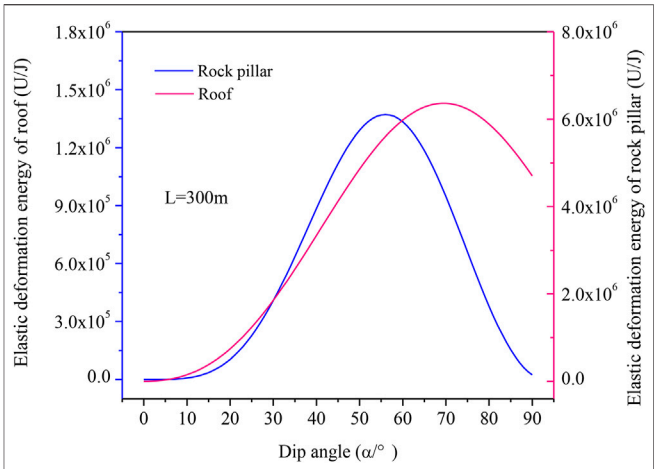

FIGURE 8 | Variation curve of the elastic deformation energy of a suspended roof and rock pillar under different dip angles (L = 300 m).

weakening and tending to stability. When the propagation distance of the vibration wave is 10 m, the normal stress decreases from 94.5 to 2.8 MPa, and the tangential stress decreases from 26.9 It can be seen that the high-energy events produced by the rock pillar fracture near the coal rock interface very easily induces a rock burst, while the high-energy events produced by the fracture at the far end of the rock pillar have difficulty inducing a rock burst. Combined with the analysis results of the previous paper, as the rock pillar is difficult to fracture as a whole, the rock burst prevention and control in the south mining area of Wudong coal mine should be based on the rock mass blasting pressure relief near the coal rock interface, supplemented by the pressure relief of the remote suspended rock pillar. At the same time, the rock pillar can be artificially fractured on site to reduce the hanging length of the rock pillar.

Mechanical Model and Elastic Deformation Energy Distribution Function of the Roof

The analysis method is the same as that in *Theoretical Analysis of Rock Bursts Induced by Stress Transfer of Hard Rock Pillar*. The roof is simplified as a cantilever beam structure mechanical model, as shown in **Figure 6**, which comprehensively considers the stress of the rock pillar. The left side of the roof is affected by the horizontal tectonic stress F_k and the gravity load G' of the overburden, which can be simplified as the load $F_4(x)$ perpendicular to the roof. The supporting force of loess on the roof of the B3+6 coal seam goaf is $F_5(x)$, and the force between the left side of the roof and coal seam is $F_6(x)$.

Assuming that the width of the roof on any section is a unit length, the load $F_4(x)$ at any position of the roof can be expressed as

$$F_4(x) = (L + l - x)\sin\alpha\left(A\gamma_s \sin\alpha + \gamma_R \cos\alpha\right) \quad (0 \le x \le L + l) \tag{15}$$

The supporting force $F_5(x)$ of loess at any section on the right side of the roof can be expressed as

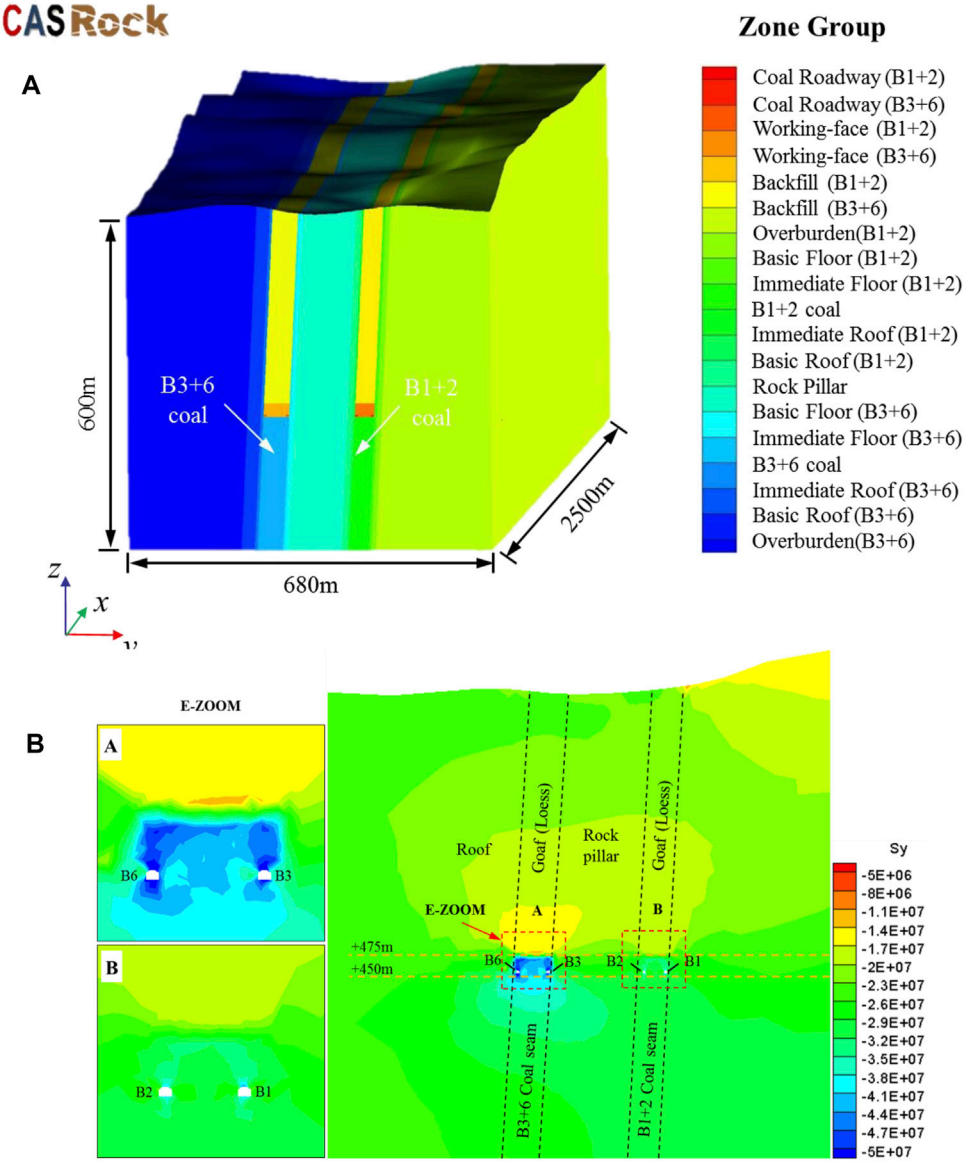

FIGURE 9 | Numerical simulation results of horizontal stress distribution in B3+6 coal seam. **(A)** Numerical calculation model; **(B)** Horizontal stress distribution of the "2.1" rock burst.

TABLE 3 | Measured tectonic stress (He et al., 2020a).

No	Level	σ_H			σ_h			σ_z		
		Stress/MPa	Trend/°	Plunge/°	Stress/MPa	Trend/°	Plunge/°	Stress/MPa	Trend/°	Plunge/°
1#	+475	15.2	158.0	15.6	10.4	70.4	8.6	8.7	188.3	72.1
2#	+475	14.1	157.3	7.8	9.6	69.2	7.8	8.4	189.4	74.8
3#	+450	15.8	158.5	15.9	10.2	76.0	15.0	9.3	193.0	69.4
4#	+450	15.4	160.5	13.6	11.3	76	8.6	9.5	178.7	65.0

σ_H *is the maximum horizontal principal stress;* σ_h *is the minimum horizontal principal stress; and* σ_z *is the vertical stress.*

TABLE 4 | Physical and mechanical property parameters of coal rock in the numerical model of the Wudong coal mine (Mine Safety Technology Branch CCRI, 2017a; Mine Safety Technology Branch CCRI, 2017b; Li et al., 2020a; He et al., 2021).

Stratum	γ KN/m^3	σ_t/MPa	σ_c/MPa	E/GPa	μ	C/MPa	Φ/°
Overburden (B1+2)	29.82	4.25	63.15	29.63	0.22	41.25	37.98
Basic Floor (B1+2)	27.50	3.01	58.11	21.70	0.25	46.57	34.20
Immediate Floor (B1+2)	26.67	4.17	49.63	18.02	0.19	32.46	38.40
B1+2 Coal Working-face (B1+2)	12.84	2.12	15.66	2.04	0.21	25.10	36.80
Immediate roof (B1+2)	20.32	3.77	30.20	26.80	0.21	35.34	33.05
Basic Roof (B1+2)	25.55	3.80	55.91	20.64	0.20	38.22	35.19
Rock Pillar	24.83	4.25	65.82	16.74	0.23	31.17	30.88
Basic Floor (B3+6)	28.87	4.39	61.12	25.91	0.22	37.66	35.10
Immediate Floor (B3+6)	27.74	4.01	57.32	20.39	0.25	33.82	36.25
B3+6 Coal Working-face (B3+6)	12.53	1.68	17.04	3.09	0.19	11.68	38.57
Immediate Roof (B3+6)	24.55	2.89	52.78	22.65	0.24	30.54	30.56
Basic Roof (B3+6)	26.85	3.66	46.90	27.56	0.22	34.22	35.91
Overburden(3+6)	27.46	4.43	58.79	21.37	0.22	21.46	36.50
Backfill (B1+2)	15.00	1.00	10.00	16.00	0.25	5.00	40.00
Backfill (B3+6)	15.00	1.00	10.00	16.00	0.25	5.00	40.00
Coal Roadway (B1+2)	12.84	2.12	15.66	2.04	0.21	25.10	36.80
Coal Roadway (B3+6)	12.53	1.68	17.04	3.09	0.19	11.68	38.57

$$F_5(x) = \frac{1}{\lambda} f\gamma_L \sin^2\alpha (L + l - x) \quad (l \le x \le L + l) \tag{16}$$

If $F_4(x)$, $F_5(x)$ and $F_6(x)$ are brought into **Eq. 5** and **Eq. 6**, the flexibility coefficient and the free term under different loads can be obtained. The uniform load of $F_6(x)$ is equivalent to the concentrated load acting on point C. The calculation results are shown in **Table 2** (only approximate calculations are made in the table).

According to Newton's third theorem, the surface load of the roof at any section is

$$F_6(x) = \frac{1}{4l}\left[F_4(x)\left(L + \frac{2}{3}l\right)^2 - q_5 L(L + 2l)\right] \tag{17}$$

According to the load distribution, the bending moment function $M(x)$ at any position along the roof can be calculated

$$M(x) = \begin{cases} (L + l - x)\left(A\gamma_s \sin^2\alpha + \gamma_R \sin\alpha\cos\alpha\right)\left[\frac{1}{6}(L + l - x)^2 - \frac{1}{4l}\left(L + \frac{2}{3}l\right)^2 (l - x)\right] \\ \quad - \frac{f\gamma_L L^3 \lambda^{-1}\sin^2\alpha}{4l}\left(x - \frac{l}{3}\right) \\ \qquad\qquad (0 \le x \le l) \\ \frac{(L + l - x)^3 \sin\alpha}{6}\left(A\gamma_s \sin\alpha + \gamma_R \cos\alpha - f\gamma_L\lambda^{-1}\sin\alpha\right) \\ \qquad\qquad (l < x \le L + l) \end{cases} \tag{18}$$

According to the relationship between the bending moment and elastic deformation energy, the elastic deformation energy at any position x along the roof can be expressed as

$$U(x) = \begin{cases} \frac{1}{2EI}\left[(L + l - x)\left(A\gamma_s \sin^2\alpha + \gamma_R \sin\alpha\cos\alpha\right)\left[\frac{1}{6}(L + l - x)^2 - \frac{1}{4l}\left(L + \frac{2}{3}l\right)^2 (l - x)\right] - \frac{f\gamma_L L^3\lambda^{-1}\sin^2\alpha}{4l}\left(x - \frac{l}{3}\right)\right]^2 \\ \qquad\qquad (0 \le x \le l) \\ \frac{1}{2EI}\left[\frac{(L + l - x)^3 \sin\alpha}{6}\left(A\gamma_s \sin\alpha + \gamma_R \cos\alpha - f\gamma_L\lambda^{-1}\sin\alpha\right)\right]^2 \\ \qquad\qquad (l < x \le L + l) \end{cases} \tag{19}$$

Under the condition of different suspended roof heights H, the variation curve of roof elastic deformation energy along the coordinate axis x direction is shown in **Figure 7A**.

Figure 7A shows that the elastic deformation energy of the roof increases with an increasing cantilever length. According to the theoretical calculation results, the elastic deformation of the roof at the interface of the B3+6 coal seam and loess can reach a maximum value. However, according to the field monitoring results (**Figure 7B**), the high-energy microseismic events of the roof are mostly concentrated in the range of 8–16 m above the working face. This is due to the stress transfer of the rock pillar and roof extrusion, the stress concentration area of the B3+6 coal seam being larger than that of the B1+2 coal seam, and the lateral restraint of coal on the roof being weakened, which leads to the downward movement of the bending position of the roof, in practice. Under the same cantilever length, the elastic deformation energy of the roof is much higher than that of the rock pillar. This is because one side of the roof directly bears the horizontal tectonic stress and the overlying load while the other side is in contact with the goaf, and the thickness of the roof

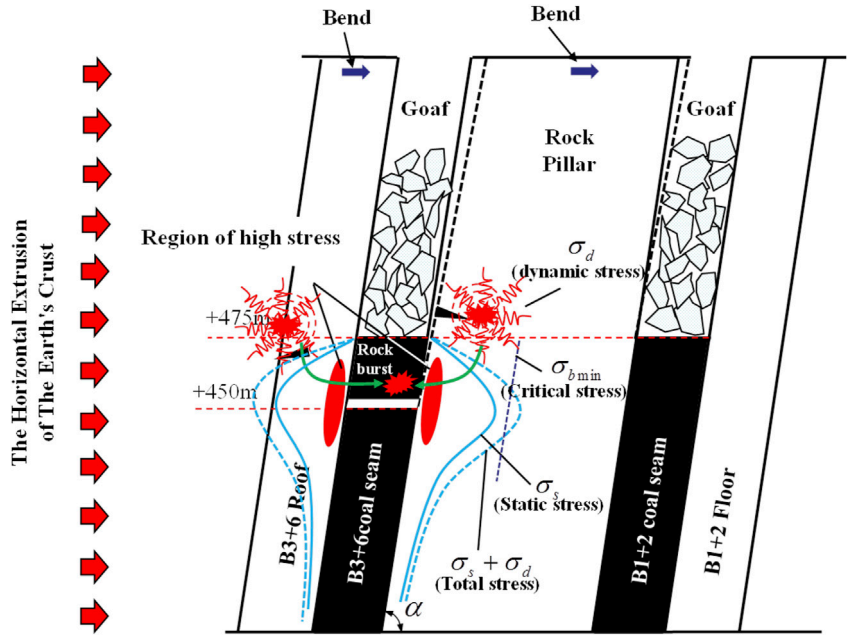

FIGURE 10 | Schematic diagram of the rock burst induced by superposition of the vibration wave load and static load.

is less than 1/2 of the rock pillar with a bending stiffness is far less than that of the rock pillar. Therefore, the roof plate is prone to bending deformation in the direction of the goaf, thus accumulating more elastic deformation energy. Both sides of the rock pillar are goaf, and the horizontal stress is greatly reduced after being attenuated by loess. The horizontal stress acting on the rock pillar is very small, which is mainly due to its own gravity bending. At the same time, the elastic strain energy of the rock pillar is relatively low due to its large thickness and large bending stiffness. Based on the statistics of the energy results of microseismic events in the period from the beginning of mining to the end of mining in B3+6 coal seam at the +450 m level (**Figure 7C**), it is determined that in the range of "10^3–10^4 J," the frequency of high-energy microseismic events in the rock pillar is much higher than that in roof, while the sum of microseismic energy of roof in the range of "10^4–10^5 J" and "$>10^6$ J" is much higher than that of rock pillar, and there is even a 10^8 J microseismic event. This is because both sides of the rock pillar are close to the working face. In the process of coal mining on both sides, compared with the roof of the B3+6 coal seam, the rock pillar will be more disturbed and release energy continuously. However, only one side of the roof is close to the working face, which is less affected by the mining disturbance, and the roof easily accumulates higher energy. Therefore, to prevent the occurrence of rock bursts in the B3+6 coal seam, roof pressure relief and artificial roof breaking are also important preventive measures. In addition, the lithology of the roof is carbonaceous mudstone. Under the condition of the same mine earthquake energy, the declining trend of the seismic wave generated after a roof fracture with distance must be the same as that of the rock pillar. Therefore, the blasting pressure relief of the roof at the coal rock junction is also an effective means to prevent rock bursts.

Influence of the Coal Seam Dip Angle on Elastic Deformation Energy

Compared with the gently inclined coal seam, the initial depth of the rock burst in the steeply inclined coal seam is smaller. Therefore, under the same geological conditions, the coal seam dip angle is also an important factor affecting the occurrence of rock bursts. When the length of the suspended roof and rock pillar is fixed, the change curve of the elastic deformation energy with the coal seam dip angle is shown in **Figure 8**. For the roof, the elastic deformation energy first increases and then decreases when the coal seam dip angle changes from 0 to 90° and reaches the maximum value when $\alpha = 69.5°$. Compared with the gently inclined coal seam, the roof of the steeply inclined coal seam has a higher elastic deformation performance. Under the same mining intensity, the rock mass is more prone to fracturing and releasing energy, which also explains why the critical depth of the rock burst in steeply inclined coal seams is much smaller than that in gently inclined coal seams. The change trend of the elastic denaturation energy of the rock pillar is the same as that of the roof. When $\alpha = 56.1°$, the elastic deformation energy of the rock pillar reaches its maximum value, but the elastic deformation energy of the roof is much greater than that of the rock pillar. This is because the goaf of the coal seam weakens the influence of horizontal *in situ* stress, and a large part of the prying force of the rock pillar comes from a gravity action rather than horizontal tectonic force, while the roof is the opposite. The bending of the roof is the result of the joint action of horizontal

tectonic force and the overlying rock mass, and its own gravity is only a small part. At the same time, the bending stiffness of the rock pillar is also greater than that of the roof, so the elastic deformation energy of the roof is much higher than that of the rock pillar under the same cantilever length.

NUMERICAL ANALYSIS

According to the results of field investigation and theoretical analysis above, the occurrence of rock bursts in subvertical extra-thick coal seams are caused by the coupling effect of roof and rock pillar. In order to verify the rationality of this analysis result, numerical analysis on the stress concentration induced by the combination of roof and rock pillar after mining was carried out. A self-developed numerical code, i.e., Cellular Automata Software for engineering the Rockmass fracturing process (CASRock), was used to simulate the stress evolution of the coal seam in the process of mining. CASRock is composed of different modulars, such as EPCA for elasto-brittle-plastic analysis, THM-EPCA for coupled thermo-hydro-mechanical analysis, RDCA for continuum-discontinuum analysis in rock mass etc. (Feng et al., 2006; Pan et al., 2009; Pan et al., 2019; Li et al., 2020b; Feng et al., 2021; Mei et al., 2021). To avoid the interference from other factors, the influence of the geological structure and mining layout is omitted in the modeling. The model is established according to the actual size of the coal seam mining area. The B3+6 coal seam is 48 m wide, the B1+2 coal seam is 37 m wide, the middle pillar is 100 m wide, the vertical direction is 600 m high, the coal seam inclination is 87°, and the coal seam strike direction is 2,500 m long. The tunnel was modeled according to the actual size. The model has a total of 76,465 elements. The actual geological conditions, incorporating thinner and weaker interlayers are simplified (**Figure 9A**). Gravity load is applied in the vertical direction with the gravity acceleration 9.8 m/s^2. The horizontal to vertical stress ratio is calibrated by field *in situ* stress measurement between levels +450 and +475 m (**Table 3**). The trapezoidal boundary stress conditions are applied and the maximum horizontal principal stress and minimum principal stress at +450 m level are around 15.6 and 10.7 MPa, respectively. After that, all boundaries except top boundary are roller fixed.

The physical and mechanical parameters of the corresponding rock strata in the model are shown in **Table 4**, and the Mohr-Coulomb strength criterion is adopted for the calculation. The mechanical parameters of coal and rock in this paper are taken according to the previous research results (Li et al., 2020a; He et al., 2021) and the technical reports from Wudong Coal Mine (Mine Safety Technology Branch CCRI, 2017a; Mine Safety Technology Branch CCRI, 2017b). In the modeling, backfilled loess and broken coal gangue in the goaf are also considered.

Take the "2.1" rock burst as an example, when a rock burst occurs, the mining level of the B3+6 and B1+2 coal seams is +450 m, and the strike positions of the working face are 1824 and 2,309 m, respectively. The simulated stress distribution is shown in **Figure 9B** (impact appearance position: 1,730 m). It can be seen that the stress of the B3+6 coal seam reaches 45.1 MPa, which is 2.64 times the uniaxial compressive strength of the coal body and 2.85 times the measured horizontal tectonic stress (mining depth of 365 m). High stress areas are found at the top and bottom of lanes B3 and B6 with the highest stress value 57.6 MPa, while at the top and bottom of lanes B1 and B2, the highest stress is only 41.2 MPa. The numerical results show that under the coupling action of rock pillar and roof, the stress concentration degree of B3+6 coal seam increases obviously, which might be the reason for the frequent occurrence of rock bursts in B3+6 coal seam. This is because the B3+6 coal seam is squeezed by a rock pillar and roof in addition to horizontal tectonic stress. The prying of the rock pillar causes a stress transfer between coal seam B1+2 and coal seam B3+6, which increases the stress of coal seam B3+6. Meanwhile, the bending of the coal seam roof to the goaf further increases the stress of the coal body. The joint action of the rock pillar and roof makes the high stress area near the B3 and B6 roadways more obvious, making it easier to produce an impact appearance.

DISCUSSION

Figure 10 shows a schematic diagram of the rock burst in the B3+6 coal seam under the coupling effect of the rock pillar and roof. The south mining area of the Wudong coal mine adopts horizontal section top coal caving, where the two adjacent coal seams are alternately mined. Due to the large dip angle of the coal seam, the roof does not easily crack. With an increasing mining depth, the stress concentration area of the B3+6 coal seam is produced under the action of the overlying rock mass and the horizontal *in situ* stress. At the same time, the release or weakening of the lateral restraint in the goaf provides deformation space for lateral deformation of the rock pillar between two coal seams. The bending and prying of the rock pillar causes the internal stress of the B3+6 coal body to increase suddenly, but the stress of the B1+2 coal seam is released. The mining stress of the B3+6 coal seam increases rapidly under the joint action of the roof and rock pillar, which provides high static stress conditions for the occurrence of rock bursts. In addition, with the mining of coal the hanging length of the roof and rock pillar of the B3+6 coal seam increases gradually. The fracture sliding of the roof and the local failure of rock pillar produce a stress wave, which makes the coal rock vibrate and rapidly increases the stress of the coal and rock mass, which provides dynamic stress conditions for the occurrence of rock burst, and ultimately leading to the occurrence of rock burst.

With an increase in the coal seam mining depth, the horizontal tectonic stress increases continuously, resulting in a stress increase of the B3+6 coal seam and B1+2 coal seam. When the mining depth is the same, the probability of a rock burst in the two coal seams should be similar. However, due to the special mining method of the near vertical extra thick coal seam, the rock pillar between the two coal seams is suspended and bent to one side of the goaf, which causes the rock pillar pry to squeeze the B3+6 coal seam and release the stress of the B1+2 coal seam (the rock pillar contains the roof of the B1+2 coal seam). At the same time, the bending compression of the roof of the B3+6 coal seam to the goaf further increases the stress of the B3+6 coal seam. Under the superposition of these three conditions, the

B3+6 coal seam is more prone to rock bursts. This is why the B3+6 coal seam is more prone to rock bursts than the B1+2 coal seam at the same mining depth.

CONCLUSION

In this paper, the mechanism of rock burst in subvertical extra-thick coal seams in the Wudong coal mine was studied using analytical and numerical methods. The main conclusions are as follows:

1) In the process of mining the B3+6 coal seam, the "inductive impact event" has an obvious regional distribution. A total of 62.5% is distributed in the rock pillar, 25.0% in the B3+6 coal seam, and 12.5% is distributed in the roof of the B3+6 coal seam. The rock pillar and B3+6 coal seam roof fractures are obvious, and the microseismic events in the energy range of 10^3–10^7 J have a concentrated distribution.
2) The mining of the B3+6 coal seam intensifies the activation of the rock pillar and leads to a more obvious prying action. The rock pillar deflects to the goaf of the B1+2 coal seam, releasing the stress of the B1+2 coal seam and increasing the stress of the B3+6 coal seam. The stress transfer of the rock pillar caused by prying is the main reason that the occurrences of rock bursts in adjacent coal seams with the same mining depth are quite different.
3) Mechanical models of the cantilever structure of the roof and rock pillar in subvertical extra-thick coal seams are established, and elastic deformation energy distribution functions are obtained. Under the same cantilever length, the elastic deformation energy of the roof is much greater than that of the rock pillar, which makes it easier to produce high-energy microseismic events. With an increasing mining depth, the roof will become the dominant factor controlling the occurrence of rock bursts.
4) The occurrence of rock bursts in the southern mining area of the Wudong coal mine is caused by the coupling action of the rock pillar prying and roof bending. Roof bending and rock pillar prying provided high static stress conditions for the occurrence of rock bursts in the B3+6 coal seam. The superposition of dynamic disturbance caused by roof and rock pillar failure and the high static stress of the coal seam is the main reason for the occurrence of rock bursts in the B3+6 coal seam.

DATA AVAILABILITY STATEMENT

The original contributions presented in the study are included in the article/supplementary material, further inquiries can be directed to the corresponding author.

AUTHOR CONTRIBUTIONS

ZW: Contribution to the paper: Data collection, Writing-original draft, Visualization. P-ZP: Contribution to the paper: Conceptualization, Supervision, Methodology. JC: Contribution to the paper: Investigation, Data collection. XL: Contribution to the paper: Methodology, Investigation. SM: Contribution to the paper: Validation, Editing. PY: Contribution to the paper: Investigation, Visualization.

FUNDING

This work was supported by National Natural Science Foundation of China (Grant Nos. 52125903, 51621006).

REFERENCES

Afraei, S., Shahriar, K., and Madani, S. H. (2019). Developing Intelligent Classification Models for Rock Burst Prediction after Recognizing Significant Predictor Variables, Section 1: Literature Review and Data Preprocessing Procedure. *Tunnelling Underground Space Technol.* 83, 324–353. doi:10.1016/j.tust.2018.09.022

Aydan, O., Genis, M., Akagi, T., and Kawamoto, T. (2002). Assessment of Susceptibility of Rock Bursting in Tunnelling in Hard Rocks. *J. Toyota Coll. Technol.* 35, 391–396. doi:10.1201/9780203746653-67

Cai, W., Bai, X., Si, G., Cao, W., Gong, S., and Dou, L. (2020). A Monitoring Investigation into Rock Burst Mechanism Based on the Coupled Theory of Static and Dynamic Stresses. *Rock Mech. Rock Eng.* 53, 5451–5471. doi:10.1007/s00603-020-02237-6

Cao, J., Dou, L., Zhu, G., He, J., Wang, S., and Zhou, K. (2020). Mechanisms of Rock Burst in Horizontal Section Mining of a Steeply Inclined Extra-thick Coal Seam and Prevention Technology. *Energies* 13, 6043. doi:10.3390/en13226043

Díez, R. R., and Álvarez, J. T. (2000). Hypothesis of the Multiple Subsidence Trough Related to Very Steep and Vertical Coal Seams and its Prediction through Profile Functions. *Geotechnical Geol. Eng.* 18, 289–311. doi:10.1023/a:1016650120053

Dou, L.-m., Mu, Z.-l., Li, Z.-l., Cao, A.-Y., and Gong, S.-y. (2014). Research Progress of Monitoring, Forecasting, and Prevention of Rockburst in Underground Coal Mining in China. *Int. J. Coal Sci. Technol.* 1, 278–288. doi:10.1007/s40789-014-0044-z

Dou, L., Cai, W., Cao, A., and Guo, W. (2018). Comprehensive Early Warning of Rock Burst Utilizing Microseismic Multi-Parameter Indices. *Int. J. Mining Sci. Technol.* 28, 767–774. doi:10.1016/j.ijmst.2018.08.007

Driad-Lebeau, L., Lahaie, F., Al Heib, M., Josien, J. P., Bigarré, P., and Noirel, J. F. (2005). Seismic and Geotechnical Investigations Following a Rockburst in a Complex French Mining District. *Int. J. Coal Geology.* 64, 66–78. doi:10.1016/j.coal.2005.03.017

Duan, H. M., Hu, X. M., and Wu, S. Z. (2008). Optimized Research on Coal Mining Method of Thin and Medium Steep Inclined Seam [J]. *Coal Sci. Technol.* 2, 16–18. doi:10.13199/j.cst.2008.02.21.duanhm.005

Feng, G.-L., Feng, X.-T., Chen, B.-R., Xiao, Y.-X., and Zhao, Z.-N. (2019). Effects of Structural Planes on the Microseismicity Associated with Rockburst Development Processes in Deep Tunnels of the Jinping-II Hydropower Station, China. *Tunnelling Underground Space Technol.* 84, 273–280. doi:10.1016/j.tust.2018.11.008

Feng, X.-T., Pan, P.-Z., and Zhou, H. (2006). Simulation of the Rock Microfracturing Process under Uniaxial Compression Using an Elasto-Plastic Cellular Automaton. *Int. J. Rock Mech. Mining Sci.* 43, 1091–1108. doi:10.1016/j.ijrmms.2006.02.006

Feng, X., Chen, B., Li, S., Zhang, C., Xiao, Y., Feng, G., et al. (2012). Studies on the Evolution Process of Rockbursts in Deep Tunnels. *J. Rock Mech. Geotechnical Eng.* 4, 289–295. doi:10.3724/sp.j.1235.2012.00289

Feng, X. T., Pan, P. Z., Wang, Z. F., and Zhang, Y. L. (2021). "Development of Cellular Automata Software for Engineering Rockmass Fracturing Processes," in International Conference of the International Association for Computer Methods and Advances in Geomechanics (Torino, Italy: Springer International Publishing). doi:10.1007/978-3-030-64514-4_4

Heib, M. A. (2012). Numerical and Geophysical Tools Applied for the Prediction of Mine Induced Seismicity in French Coalmines. *Ijg* 03, 834–846. doi:10.4236/ijg.2012.324084

He, J., and Dou, L.-M. (2012). Gradient Principle of Horizontal Stress Inducing Rock Burst in Coal Mine. *J. Cent. South. Univ.* 19, 2926–2932. doi:10.1007/s11771-012-1360-3

He, J., Dou, L., Gong, S., Li, J., and Ma, Z. (2017). Rock Burst Assessment and Prediction by Dynamic and Static Stress Analysis Based on Micro-seismic Monitoring. *Int. J. Rock Mech. Mining Sci.* 93, 46–53. doi:10.1016/j.ijrmms.2017.01.005

He, M. (2011). Physical Modeling of an Underground Roadway Excavation in Geologically 45° Inclined Rock Using Infrared Thermography. *Eng. Geology.* 121, 165–176. doi:10.1016/j.enggeo.2010.12.001

He, S., Chen, T., Vennes, I., He, X., Song, D., Chen, J., et al. (2020a). Dynamic Modelling of Seismic Wave Propagation Due to a Remote Seismic Source: A Case Study. *Rock Mech. Rock Eng.* 53, 5177–5201. doi:10.1007/s00603-020-02217-w

He, S., Song, D., He, X., Chen, J., Ren, T., Li, Z., et al. (2020b). Coupled Mechanism of Compression and Prying-Induced Rock Burst in Steeply Inclined Coal Seams and Principles for its Prevention. *Tunnelling Underground Space Technol.* 98, 103327. doi:10.1016/j.tust.2020.103327

He, X. Q., Chen, J. Q., Song, D. Z., He, S. Q., Li, Z. L., Zhong, T. P., et al. (2021). Study on Mechanism of Rock Burst and Early Warning of Typical Steeply Inclined Coal Seams. *Coal Sci. Technol.* 49, 13–22. doi:10.13199/j.cnki.cst.2021.06.002

Kaiser, P. K., and Cai, M. (2013). "Critical Review of Design Principles for Rock Support in Burst-Prone Ground-Time to Rethink," in Seventh International Symposium on Ground Support in Mining & Underground Construction, Perth, WA, October 5–8, 2009. Editors Potvin Y. and Brady B. (Perth, WA: Australian Centre for Geomechanics), 3–38. doi:10.36487/ACG_rep/1304_01_Kaiser

Lai, X. P., Sun, H., Shan, P. F., Cai, M., Cao, J. T., and Feng, C. (2015). Structure Instability Forecasting and Analysis of Giant Rock Pillars in Steeply Dipping Thick Coal Seams. *Int. J. Minerals, Metall. Mater.* 22, 1223. doi:10.1007/s12613-015-1190-z

Lai, X. P., Yang, Y. R., Wang, N. B., Shan, P. F., and Zhang, D. S. (2018). Comprehensive Analysis to Temporal-Spatial Variation of Dynamic Instability of Steeply Inclined Coal-Rock Mass. *Chin. J. Rock Mech. Eng.* 37, 583–592. doi:10.13722/j.cnki.jrme.2017.1115

Lai, X., Shan, P., Cao, J., Sun, H., Suo, Z., and Cui, F. (2014). Hybrid Assessment of Pre-Blasting Weakening to Horizontal Section Top Coal Caving (HSTCC) in Steep and Thick Seams. *Int. J. Mining Sci. Technol.* 24, 31–37. doi:10.1016/j.ijmst.2013.12.006

Li, D. H., He, X. Q., Chen, J. Q., Song, D. Z., Li, Z. L., He, S. Q., et al. (2020a). Inducing Mechanism of Rockburst Occurring in Steeply-Inclined Coal Seam of Wudong Coal Mine. *J. China Univ. Mining Technol.* 49, 835–843. doi:10.13247/j.cnki.jcumt.001191

Li, M., Mei, W., Pan, P.-Z., Yan, F., Wu, Z., and Feng, X.-T. (2020b). Modeling Transient Excavation-Induced Dynamic Responses in Rock Mass Using an Elasto-Plastic Cellular Automaton. *Tunnelling Underground Space Technol.* 96, 103183. doi:10.1016/j.tust.2019.103183

Liu, C., Li, H., Mitri, H., Jiang, D., Li, H., and Feng, J. (2017). Voussoir Beam Model for Lower strong Roof Strata Movement in Longwall Mining - Case Study. *J. Rock Mech. Geotech. Eng.* 9, 1171–1176. doi:10.1016/j.jrmge.2017.07.002

Lu, C.-P., Liu, G.-J., Zhang, N., Zhao, T.-B., and Liu, Y. (2016). Inversion of Stress Field Evolution Consisting of Static and Dynamic Stresses by Microseismic Velocity Tomography. *Int. J. Rock Mech. Mining Sci.* 87, 8–22. doi:10.1016/j.ijrmms.2016.05.008

Mazaira, A., and Konicek, P. (2015). Intense Rockburst Impacts in Deep Underground Construction and Their Prevention. *Can. Geotech. J.* 52, 1426–1439. doi:10.1139/cgj-2014-0359

Mei, W., Li, M., Pan, P.-Z., Pan, J., and Liu, K. (2021). Blasting Induced Dynamic Response Analysis in a Rock Tunnel Based on Combined Inversion of Laplace Transform with Elasto-Plastic Cellular Automaton. *Geophys. J. Int.* 225, 699–710. doi:10.1093/gji/ggaa615

Miao, S. J., Lai, X. P., and Cui, F. (2011). Top Coal Flows in an Excavation Disturbed Zone of High Section Top Coal Caving of an Extremely Steep and Thick Seam. *Mining Sci. Technol.* 21, 99–105. doi:10.1016/j.mstc.2010.12.006

Mine Safety Technology Branch CCRI (2017a). *Appraisal Report on Bursting Liabilityof B1 + 2 Coal Seam and its Roof and Floor in Wudong Coal Mine.* Urumqi: Group XECoSE.

Mine Safety Technology Branch CCRI (2017b). *Appraisal Report on Bursting Liabilityof B3 + 6 Coal Seam and its Roof and Floor in Wudong Coal Mine.* Urumqi: Group XECoSE.

Naji, A. M., Emad, M. Z., Rehman, H., and Yoo, H. (2019). Geological and Geomechanical Heterogeneity in Deep Hydropower Tunnels: A Rock Burst Failure Case Study. *Tunnelling Underground Space Technol.* 84, 507–521. doi:10.1016/j.tust.2018.11.009

Pan, P.-Z., Yan, F., Feng, X.-T., Wu, Z., and Qiu, S. (2019). Modeling of an Excavation-Induced Rock Fracturing Process from Continuity to Discontinuity. *Eng. Anal. Bound. Elem.* 106, 286–299. doi:10.1016/j.enganabound.2019.05.014

Pan, P. Z., Feng, X. T., and Zhou, H. (2009). Failure Evolution Processes of Brittle Rocks Using 3D Cellular Automaton Method. *Rock Soil Mech.* 30, 1471–1476. doi:10.16285/j.rsm.2009.05.054

Qi, Q. X., Li, Y. Z., Zhao, S. K., Pan, P. Z., and Wei, X. Z. (2019a). Discussion on the Mechanism and Control of Coal Bump Among Mine Group. *J. China Coal Soc.* 44, 141–150. doi:10.13225/j.cnki.jccs.2018.1701

Qi, Q. X., Li, Y. Z., Zhao, S. K., Zhang, N. B., Zheng, Y. W., Li, H. T., et al. (2019b). Seventy Years Development of Coal Mine Rockburst in China: Establishment and Consideration of Theory and Technology System. *Coal Sci. Technol.* 47, 1–35. doi:10.13199/j.cnki.cst.2019.09.001

Simser, B. P. (2019). Rockburst Management in Canadian Hard Rock Mines. *J. Rock Mech. Geotechnical Eng.* 11, 1036–1043. doi:10.1016/j.jrmge.2019.07.005

Unver, B., and Yasitli, N. E. (2006). Modelling of Strata Movement with a Special Reference to Caving Mechanism in Thick Seam Coal Mining. *Int. J. Coal Geology.* 66, 227–252. doi:10.1016/j.coal.2005.05.008

Wang, H., Shi, R., Deng, D., Jiang, Y., Wang, G., and Gong, W. (2020). Characteristic of Stress Evolution on Fault Surface and Coal Bursts Mechanism during the Extraction of Longwall Face in Yima Mining Area, China. *J. Struct. Geology.* 136, 104071. doi:10.1016/j.jsg.2020.104071

Wang, Z. Y., Dou, L. M., Wang, G. F., Feng, L. F., Kang, K., Bai, J. Z., et al. (2018). Resisting Impact Mechanical Analysis of an Anchored Roadway Supporting Structure under P-Wave Loading and its Application in Rock Burst Prevention. *Arab. J. Geosci.* 11, 1–18. doi:10.1007/s12517-018-3426-5

Wu, Y. P., Liu, K. Z., Yun, D. F., Xie, P. S., and Wang, H. W. (2014). Research Progress on the Safe and Efficient Mining Technology of Steeply Dipping Seam. *J. China Coal Soc.* 39, 1611–1618. doi:10.13225/j.cnki.jccs.2014.9039

Wu, Z. H., Pan, P. Z., Pan, J. F., Wang, Z. F., and Gao, J. M. (2021a). Analysis on Mechanism of Rock Burst and Law of Mine Earthquake Activity in Graben Structural Area. *Rock Soil Mech.* 42, 2225–2238. doi:10.16285/j.rsm.2020.1732

Wu, Z. H., Pan, P. Z., Zhao, S. K., Liu, X. D., Miao, S. T., and Li, Y. Z. (2021b). Study on the Mechanism of Rock Bursts Caused by "Roof-Rock Pillar"in Mining Steeply-Inclined and its Prevention and Treatment. *J. China Coal Soc.* 46 (S1), 49–62. doi:10.13225/j.cnki.jccs.2020.0916

Xu, J., Jiang, J., Xu, N., Liu, Q., and Gao, Y. (2017). A New Energy index for Evaluating the Tendency of Rockburst and its Engineering Application. *Eng. Geology.* 230, 46–54. doi:10.1016/j.enggeo.2017.09.015

Xu, S. M., Li, S. Y., Li, D. X., Zhang, W. P., Lian, J., and Wei, Q. D. (2015). Geological Laws of Rock Burst Occurrence in Yima coalfield. *J. China Coal Soc.* 40, 2015–2020. doi:10.13225/j.cnki.jccs.2015.0715

Zhu, S., Feng, Y., and Jiang, F. (2015). Determination of Abutment Pressure in Coal Mines with Extremely Thick Alluvium Stratum: A Typical Kind of Rockburst Mines in China. *Rock Mech. Rock Eng.* 49, 1943–1952. doi:10.1007/s00603-015-0868-x

Conflict of Interest: Author JC was employed by the company Shenhua Xinjiang Energy Company Limited.

The remaining authors declare that the research was conducted in the absence of any commercial or financial relationships that could be construed as a potential conflict of interest.

Publisher's Note: All claims expressed in this article are solely those of the authors and do not necessarily represent those of their affiliated organizations, or those of the publisher, the editors and the reviewers. Any product that may be evaluated in this article, or claim that may be made by its manufacturer, is not guaranteed or endorsed by the publisher.